Meteorol Atmos Phys (2009) 105:69–83
DOI 10.1007/s00703-009-0034-7

ORIGINAL PAPER

Space-time structures of earthquakes

T. N. Krishnamurti · Ruby Krishnamurti · Anitha D. Sagadevan · Arindam Chakraborty · William K. Dewar · Carol Anne Clayson · James F. Tull

Received: 11 November 2008 / Accepted: 28 February 2009 / Published online: 13 August 2009

Abstract Using the United States Geological Survey global daily data sets for 31 years, we have tabulated the earthquake intensities on a global latitude longitude grid and represented them as a finite sum of spherical harmonics. An interesting aspect of this global view of earthquakes is that we see a low frequency modulation in the amplitudes of the spherical harmonic waves. There are periods when these waves carry larger amplitudes compared to other periods. A power spectral analysis of these amplitudes clearly shows the presence of a low frequency oscillation in time with a largest mode around 40 days. That period also coincides with a well-know period in the atmosphere and in the ocean called the Madden Julian Oscillation. This paper also illustrates the existence of a spatial oscillation in strong earthquake occurrences on the western rim of the Pacific plate. These are like pendulum oscillations in the earthquake frequencies that swing north or south along the western rim at these periods. The spatial amplitude of the oscillation is nearly 10,000 km and occurs on an intraseasonal time scale of 20–60 days. A 34-year long United States Geological Survey earthquake database was examined in this context; this roughly exhibited 69 swings of these oscillations. Spectral analysis supports the intraseasonal timescale, and also reveals higher frequencies on a 7–10 day time scale. These space-time characteristics of these pendulum-like earthquake oscillations are similar to those of the MJO. Fluctuations in the length of day on this time scale are also connected to the MJO. Inasmuch as the atmospheric component of the MJO will torque the solid earth through mountain stresses, we speculate the MJO and our proposed earthquake cycle may be connected. The closeness of these periods calls for future study.

T. N. Krishnamurti (✉) · A. D. Sagadevan · A. Chakraborty · C. A. Clayson
Department of Meteorology, Florida State University, Tallahassee, FL, USA
e-mail: tkrishnamurti@fsu.edu

R. Krishnamurti · W. K. Dewar
Department of Oceanography, Florida State University, Tallahassee, FL, USA

R. Krishnamurti · C. A. Clayson
Geophysical Fluid Dynamics Institute, Florida State University, Tallahassee, FL, USA

J. F. Tull
Department of Geological Sciences, Florida State University, Tallahassee, FL, USA

Present Address:
A. Chakraborty
Centre for Atmospheric and Oceanic Sciences, Indian Institute of Science, Bangalore, India

1 Introduction

This paper examines global earthquake data sets in a planetary space-time context, and illustrates some interesting aspects that have been overlooked in the past. Plate tectonic theory presents only a statistical, special (geographic) and otherwise static picture of earthquake occurrences. The search for precursors of individual events is usually studied on the local scale within a single fault system. The interrelationship of global and local scales has generally received less attention, but is the focus here. It was noted by Knopoff (1996) that "an ability to predict earthquakes either on an individual basis or on a statistical basis remains remote. It is clear that scientific issues must be understood before routine prediction can be announced". Today, a decade later, earthquake prediction

is still remote, but great progress appears to have been made on the scientific issues. Whereas weak earthquakes (magnitude <3) show self-similarity with no detectable length scale, strong earthquakes do have a length scale associated with their seismicity. Strong earthquakes (magnitude ≥5) are those that rupture a significant area along lithosphere-bounding faults (Sykes 1996). They have seismicity related to inhomogeneities with characteristic length scales on the order of 100 m, according to Aki (1996), who utilized coda wave interferometry. Coda waves are late-arriving seismic waves (like the coda signifying the end of a musical composition). Whereas, the early (direct) arrivals may show no detectable effect of small changes in the medium, coda waves represent those scattered by inhomogeneities and these would have repeatedly sampled the medium. Thus, coda wave interferometry has been used successfully in varied applications such as to detect changes in volcanic activity on a two-day time lapse (Gret et al. 2006), and to infer weakening of faults and asperities by the injection of fluids.

Aki's (1996) analysis on coda waves (late-arriving seismic waves) trapped in fault zones, describes the process as a creep flow in the lower plastic part of the fault which allows for stress release, while in the brittle upper part there is no stress release. It is the stress release in the brittle zone that causes seismicity.

Kanamori (1981) used a space-time display of earthquakes surrounding major seismic events, for the purpose of showing the nature of precursors. Long periods, often of several years duration having notable quiescence, were shown to precede many major earthquakes. The time scales of 30–60 days, which are our focus here, were not resolved in those presentations. A relationship between atmospheric pressure field and earthquake occurrences over California was shown by Namias (1988, 1989).

1.1 The USGS earthquake data sets

The United States Geological Survey (USGS) is a leading geological organization allied with seismograph stations around the world which receives, analyzes, maintains, and distributes data on earthquake activity worldwide. This historical (USGS) earthquake data base provides information on the time, location, depth, and magnitude of the earthquakes from 2100 B.C. to the present. The data base contains earthquakes with known magnitude values between 0.1 and 9.9. Here, we consider earthquakes along the western rim of the Pacific plate during the years 1973–2006 as recorded in the (USGS) earthquake database. The convergent plate boundaries of the western Pacific clearly stand out in this distribution as can be seen in Fig. 1a. These data were binned into the roughly 1,000-km squares shown in Fig. 1b, and over temporal intervals of 3 days,

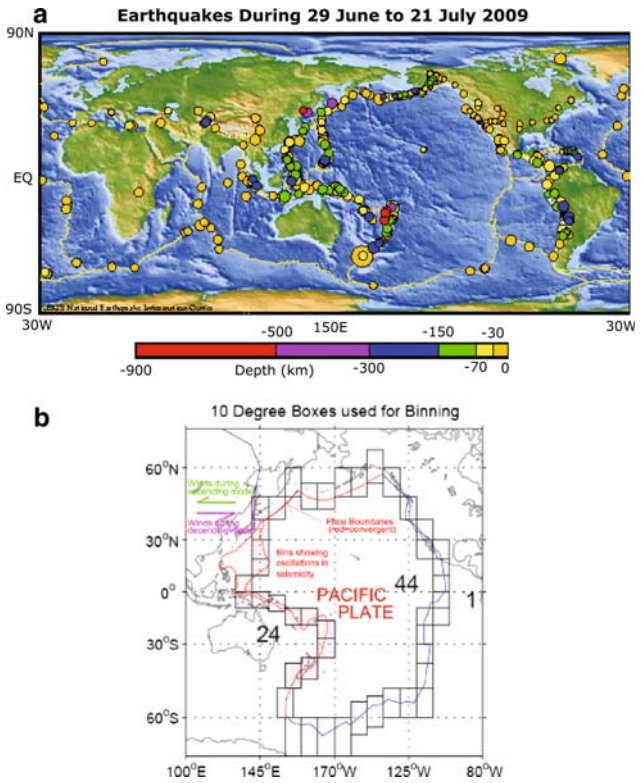

Fig. 1 **a** Earthquake intensities plotted during 30 June to 21 July 2009 as obtained from http://neic.usgs.gov/neis/qed/; **b** 10° latitude/longitude bins were used for the data analysis

retaining only events of magnitude ≥5 on the Richter scale. Such space-time binning was necessary given the spatially sporadic nature of earthquake epicenters.

1.2 Global time scales

If one takes the global distributions of earthquakes for a given day, that data set can be expressed in the global context by expanding their intensities using spherical harmonics. Most places, devoid of earthquakes, will carry a number zero for the intensity, whereas along or near the lithospheric plate boundaries there can be many places that carry non-zero numbers. This representation calls for an initial tabulation of these zeros and non-zeros on a global latitude/longitude grid. The spherical harmonic representation requires a grid to spectral transformation. That finite representation of data is highly revealing in showing that the earthquakes do carry space-time scales similar to many other geophysical problems. The finite representation is described by a discrete set of spherical harmonics such that the input field is completely recovered (except for minor problems at the edge of zeros and adjacent large non-zero numbers, called the Gibbs phenomena). Figure 2a shows the earthquake distributions on a given day. Figure 2c, d shows the positive and negative spectral amplitudes

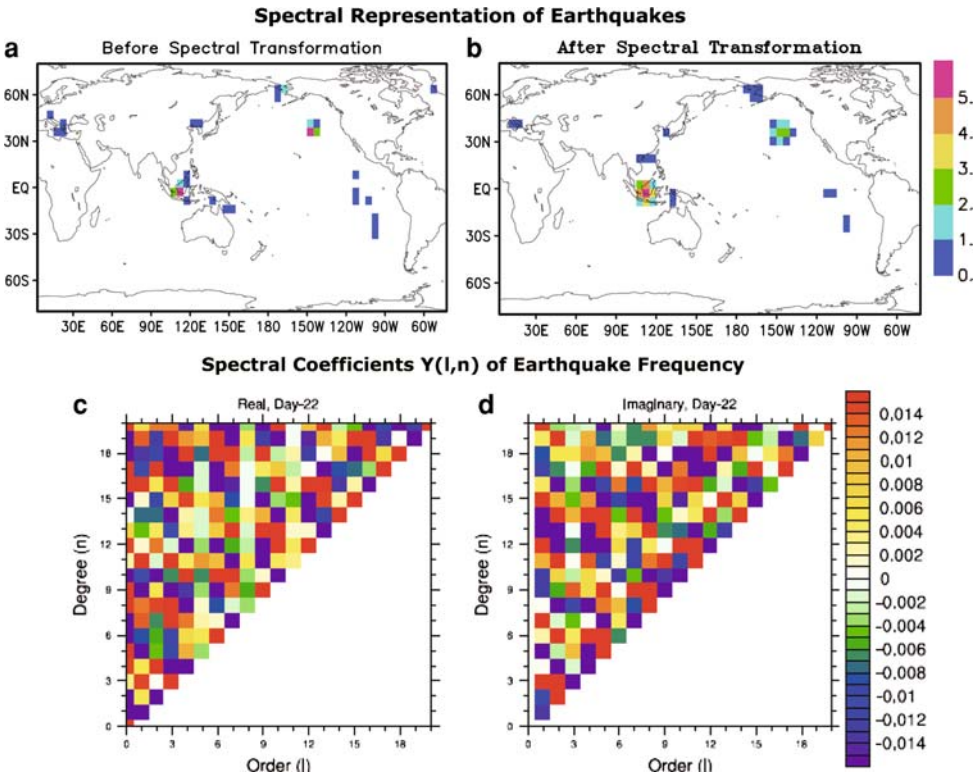

Fig. 2 **a** The distribution of earthquake intensities on a random date. **b** Backward transform results from spectral to grid, showing the rerecorded earthquake distribution. **c** Real, **d** Imaginary parts of the 2-D harmonic coefficients conducted for digitizing **a**. Here, ordinate: degree of associate Legendre polynomials; abscissa: order of trigonometric waves in the zonal direction

(triangular truncation) for this data decomposition into spherical harmonics. This is called a Fourier Legendre transform of the input data. An inverse transform is next performed to see the recovery of the input data for the spectral coefficients. That recovery shown in Fig. 2d matches closely with the input data of Fig. 2a. The differences, if any, arise due to what is called a Gibbs phenomenon, when we expand spatial data sets with sharp changes such as a zero and large non-zero values adjacent to each other. The Gibbs phenomenon is not severe and we are able to replicate the initial field nearly exactly by this finite representation from 2-D waves. This aspect has been tested in the same way as we do in atmospheric spectral modeling, (Krishnamurti et al. 2007). We show these to emphasize that the entire set of spectral coefficients is an useful mathematical representation for the global earthquake of that day. We will next look at this global representation of these data sets.

In order to look at the salient time scales of the global earthquake data sets, we have performed a spectral analysis of the daily mean spectral amplitude data sets, covering the years (1973 to 2004) that includes all spatial scales in two dimensions. The time series of these global amplitudes are shown in Fig. 3. They are the vector sums of amplitudes of the real and imaginary parts for all of the spherical harmonics. In this analysis, we have only included the averaging for the first 20 spherical harmonic waves. The time series of what can be called a "daily earthquake index" seems to show interesting features on many time scales. There are often peaks that are values separated by tens of days and some that seem to occur at more rapid intervals. A spectral analysis of this data set is shown in Fig. 4. This covers the power spectra for the entire period of 32 years and also some at 3-year intervals. Also included in these illustrations are the lines defining the confidence limits at 95 and 99% levels and the red noise spectra. Here, we see some peaks in the spectral variances at high frequencies (less than 10 days), there are also some marked peaks in the time scales especially around 40 days and higher. These can be seen in the spectra for the 32-year long data sets as well in the three yearly segments illustrated here. A peak around 40 days in the spectra based on 32-year long data set carries the largest variance.

When we look at a sequence of global spectral amplitudes for each of the spherical harmonics, we see an interesting alternation in the magnitudes with time. There are periods when these amplitudes in general are all small and there are periods when they are all quite large in comparison. In Fig. 5a, b and c, we show a 116-day sequence of these at intervals of 5 days. Here, the red and purple colorings denote larger amplitudes, and yellow and green denote smaller amplitudes on the color scale (also indicated). The amplitudes of the real and imaginary parts of global representation of the earthquakes are shown here. This display

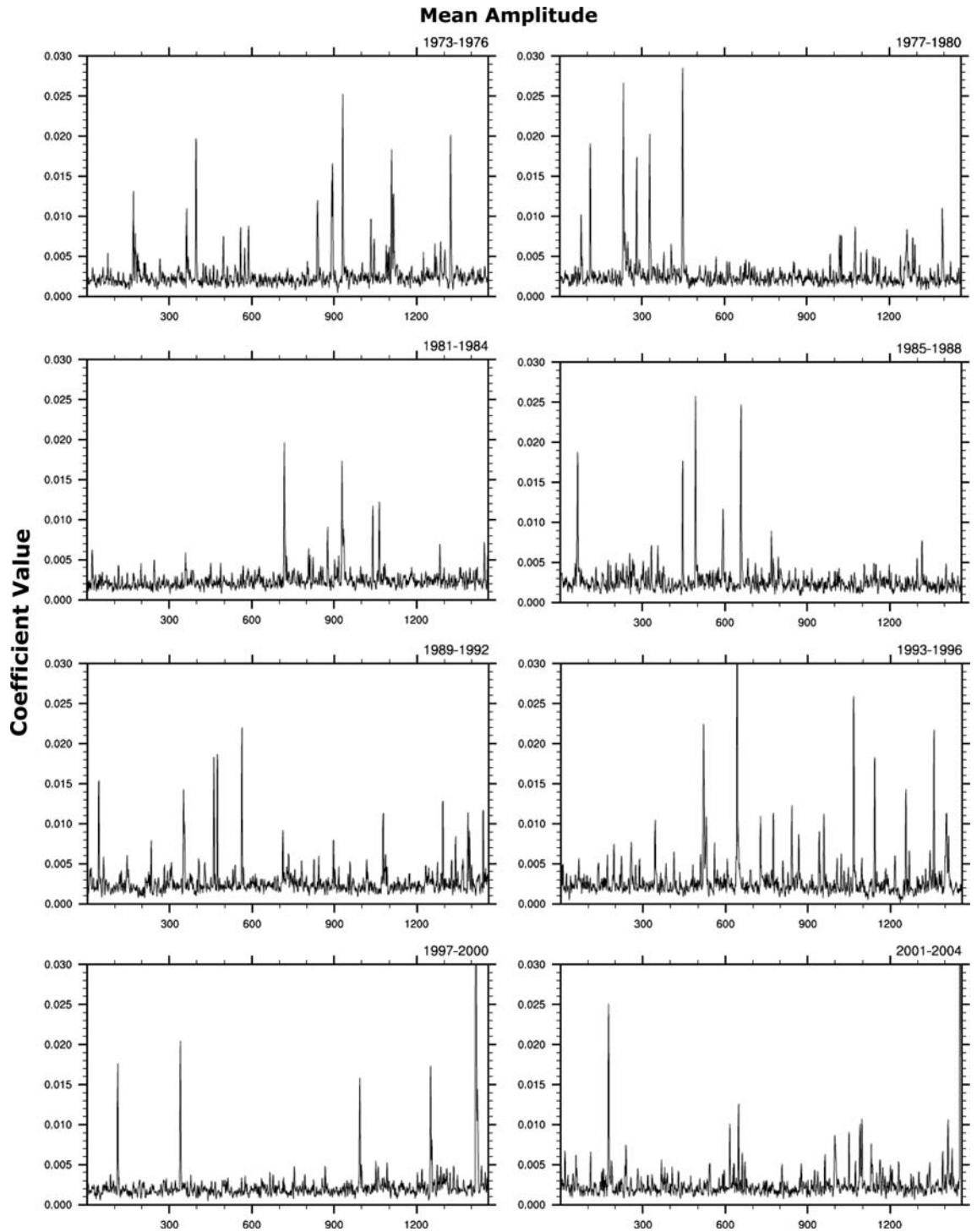

Fig. 3 Daily vector summed amplitude of global earthquake for 4-year segment covering 32 year. Here, ordinate: vector summed amplitude; abscissa: time in days

suggests a low frequency oscillation in the global amplitudes for most of the waves in this spherical harmonic representation. What this implies is that there are days with large amplitudes for a large number of global spherical harmonic components that describe the earthquakes, and then there are days when the global earthquakes are described by waves of smaller amplitudes. The same data set confirmed, as shown in Fig. 4, that there exists a dominant 40-day oscillation in the global earthquake activity. These amplitude displays of Fig. 4 merely confirms that finding.

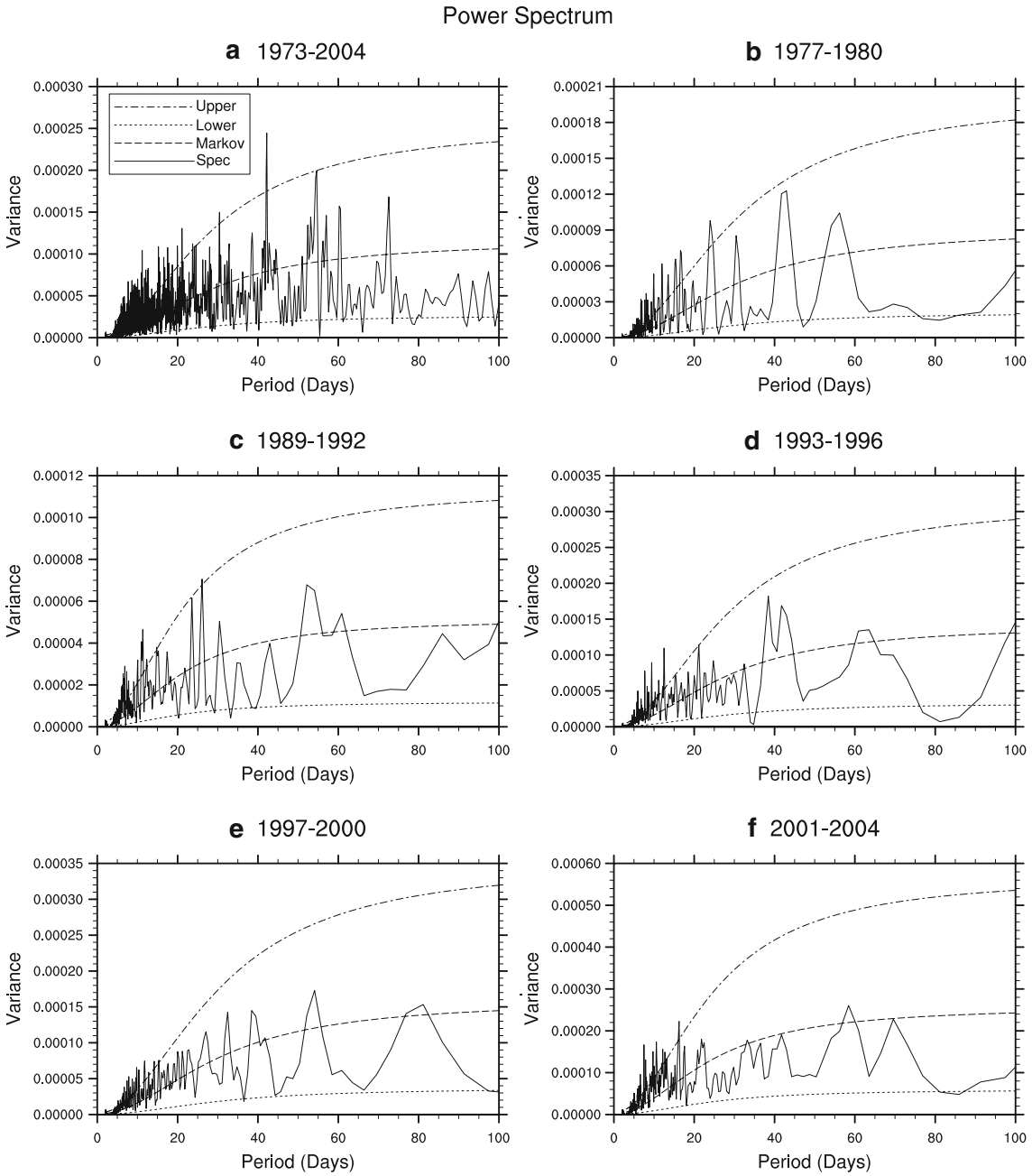

Fig. 4 Power spectra as a function of period. Here, ordinate: power times the frequency; abscissa: periods in days

1.3 The Madden Julian Oscillation

There has been a considerable amount of research on a slow eastward moving wave called the Madden Julian Oscillation (MJO) in the earth's atmosphere. This wave has a scale of nearly 10,000 km and traverses around the earth in roughly 20–60 days (Madden and Julian 1971, 1972). This wave has its largest amplification in the equatorial latitudes. This wave carries a disturbed and an undisturbed part as it propagates, such that roughly one half of this wave includes cloudy and disturbed weather. Within this disturbed part one sees a plethora of cumulonimbus rain producing clouds. Nakazawa (1988) emphasized an envelope of this disturbed part of the MJO wave that moves west to east whereas the individual cloud elements within it often move in a different direction compared to that of the envelope. In the course of looking at space-time data sets of strong earthquakes with intensity ≥ 5 on the Richter scale, related to the convergent plate boundaries along the western rim of the Pacific plate, we noted the possibility of illustrating a large-scale envelope of earthquake occurrences. That envelope carries a number of individual earthquakes whose position of precise

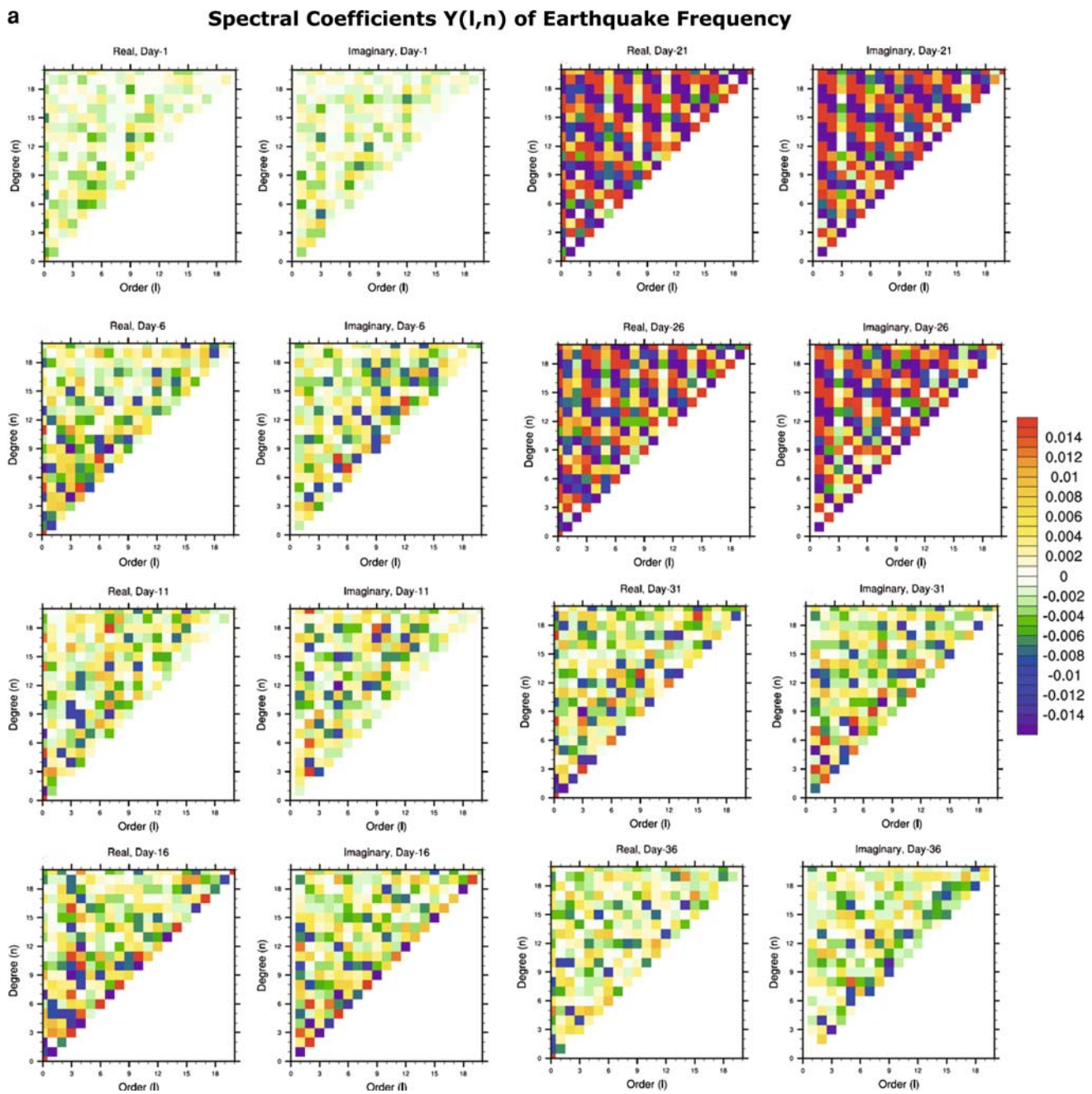

Fig. 5 This illustration shows the 2-D amplitude (real and imaginary parts) of global earthquake expressed by spherical harmonic waves. Here, ordinate: degree of associate Legendre polynomials; abscissa: order of trigonometric waves in the zonal direction. Different panels show a sequence of 116 plots at interval of 5 days

occurrence would be difficult to predict. The clouds within the Nakazawa envelope, illustrated in Fig. 6, are difficult to predict but the envelope's motion has been predicted by many authors, e.g., Krishnamurti et al. (2007). The main objective of this paper is to illustrate an earthquake occurrence envelope using some 32 years of data and to draw some parallels with the MJO, both of which seem to carry similar time scales.

Figure 6 is based on the findings of Nakazawa (1988). This is a longitude/time diagram called the Hovmoller diagram. This shows envelopes of cloud elements that propagate from west to east in periods roughly of the order of 20–60 days. This is called the Madden Julian wave. There is a disturbed (cloudy) part of this wave and a relatively quiescent part of this wave, these are identified in this illustration. The cloud elements inside the envelope

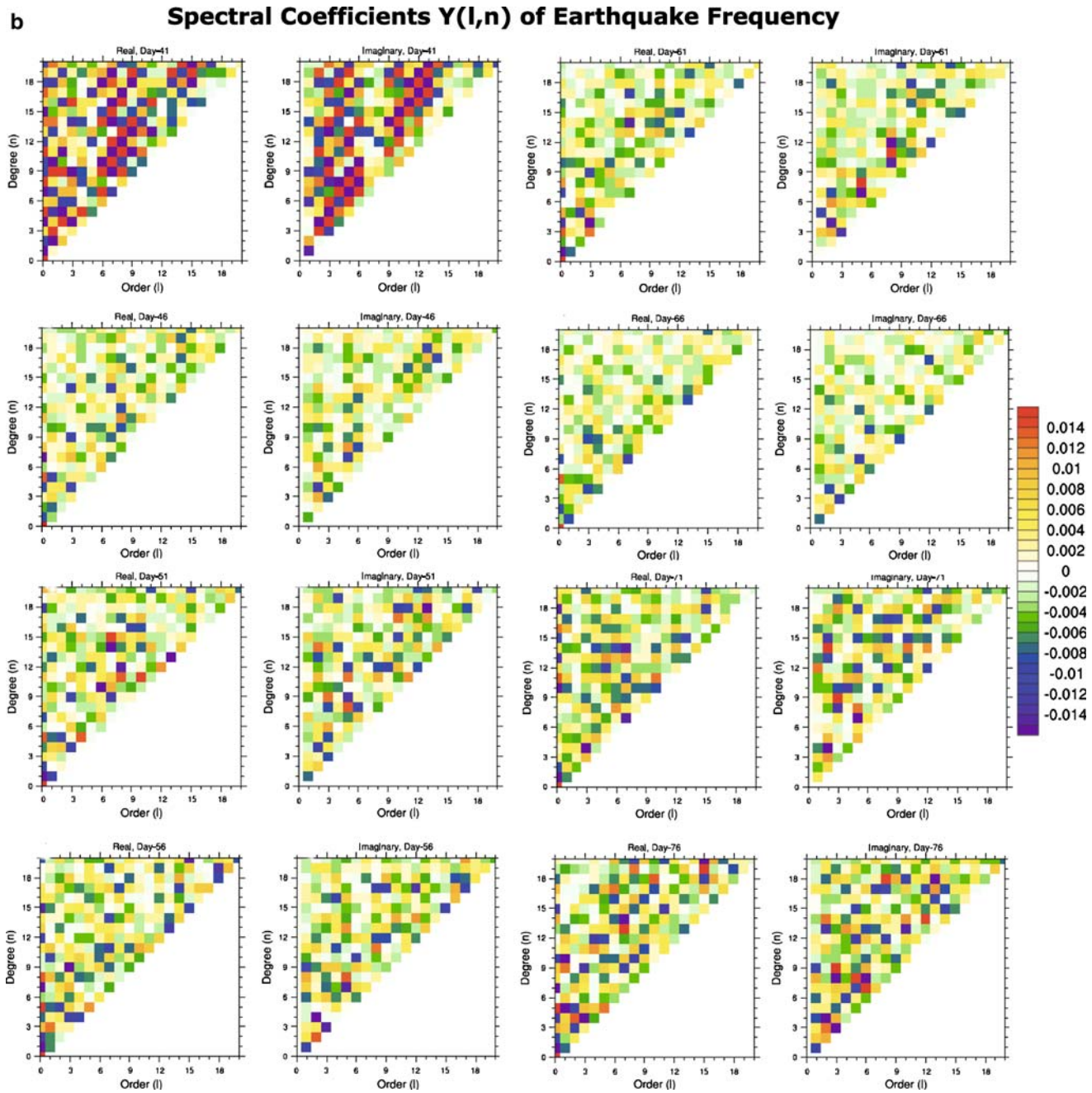

Fig. 5 continued

generally propagate westwards at a speed of around 500–700 km/day. An important point that meteorologists recognize is that it is very difficult to predict where and when a single cloud might next form within the cloudy part of the envelope, although the envelope has its own identity. We shall illustrate that somewhat similar space-time diagrams can be constructed to illustrate active and relatively inactive earthquake occurrences along the western Pacific rim. Here, again the goal is not to predict where and when of a single event.

2 The space-time organization of earthquakes on the western Pacific rim

Figure 7a illustrates the space-time evolution of earthquake occurrence along the western Pacific rim during a 100-day period beginning in July, 1983. The abscissa represents the boxes numbered in Fig. 1b with box number 24 denoting roughly the center of the western rim and also the location of the greatest activity over the last 32 years. In this illustration (Fig. 7a), the dark stipplings are regions where

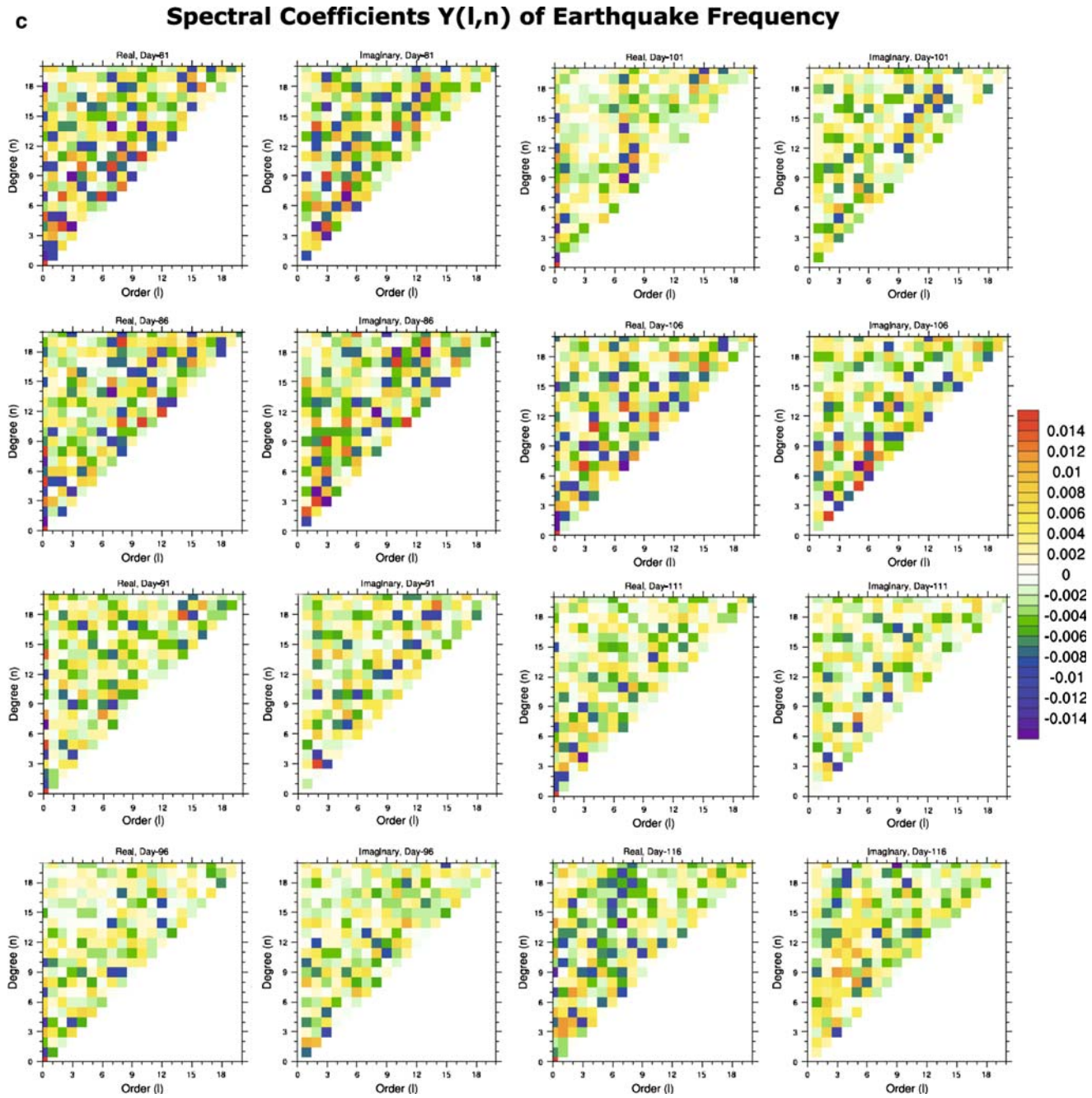

Fig. 5 continued

more than one earthquake occurrence was noted within each of the space-time bins. The stippling utilizes a cubic rule, i.e., 2 earthquakes are represented by 8 dots, 3 by 27 dots and so on. This was done to see a space-time pattern of major earthquakes. What one notices in Fig. 7a is the tendency for earthquake occurrences to swing first toward the southern tip of the rim (boxes less than 24) and then back to the northern tip (boxes greater than 24, Fig. 1b). This repeats for roughly two and one half cycles over the 100-day interval, yielding a roughly 40-day time scale. An ovular envelope is plotted on the figure to track the oscillation. This envelope's shape was arrived at after analyzing nearly 100 such illustrations from the last 34 years of data sets. The lateral extent of this feature is nearly 10,000 km. In Fig. 7a, we also display a line (red color) that connects the 3-day maxima of earthquake activity. This is an alternate representation for the oscillation presented in this study. This diagram describes traveling waves of

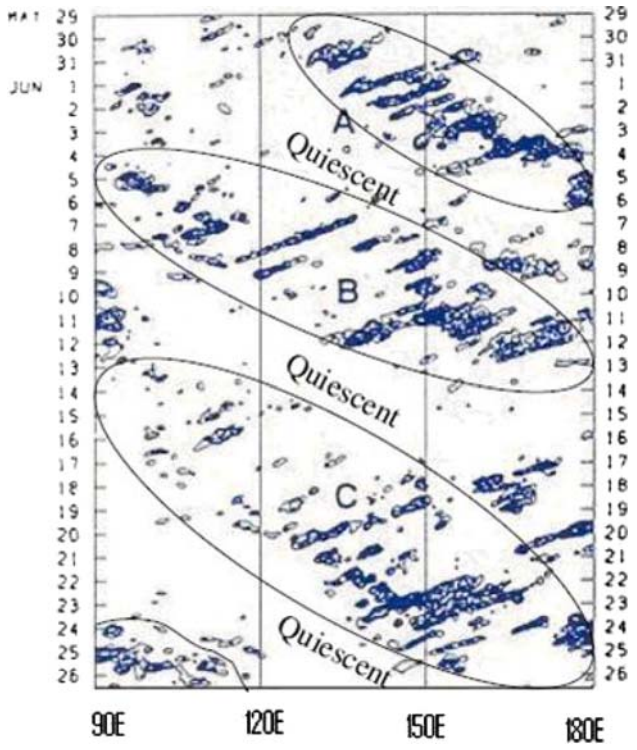

Fig. 6 An x-t (longitude/time) diagram of the clouds over (as seen from infrared brightness) for a polar orbiting satellite. Data, meridionally averaged between the equator and 5°N are shown. This covers the period May and June of 1980. Longitudes are shown along abscissa. The envelopes (**a**, **b,** and **c**) show ellipse enclose active cloudy periods while they are separated by quiescent periods

earthquake occurrences that spans the entire western Pacific rim. It is the recognition of this apparently organized earthquake behavior that is the major contribution of this paper.

A connection of events by the straight-line segments in Fig. 7a is not meant to be deterministic. Our emphasis here will be on the oscillation of an envelope that carries several events in space-time.

Figure 7b, c and d includes several more examples of this pendulum-like swing. Here, the frequency of occurrences of major earthquakes is represented by the corresponding numbers in color. A total of 69 such oscillations were found during the 32 years period between 1973 and 2006. The envelope is again provided to facilitate the viewing of the phenomenon. It is important to note that the envelope represents special propagation of regions of enhanced earthquake probability, not earthquakes per se. Within the envelope, there are many locations along the plate boundary where no major earthquake activity occurs. A time series analysis of the earthquake occurrences sees periods of the order of 20–60 days for the farthest displacement points of the pendulum-like swings of earthquake occurrences (Fig. 8).

3 Possible relationship of atmospheric to solid earth phenomena

The Earth's rigid lithospheric plates move across a deformable zone (asthenosphere) in the underlying upper mantle driven principally by complex convective motions, and interact along plate boundaries via faulting and other modes of deformation. Wind-forced mountain torques which cyclically alter earth's angular momentum add an additional oscillating force component across mountainous continental plates, and thus a small oscillating compressional/extensional stress component to plate-bounding fault systems. The amplitude of the oscillation of mountain torques derived from surface pressure data produces an oscillating horizontal force of $\sim 1.6 \times 10^{12}$ N across Asia.

A composite structure of the atmospheric low frequency winds (on the time scale of 20–60 days) at 850-hPa level for the respective clockwise (ascending) and the counterclockwise (descending) swings of the earthquake pendulum are shown in Fig. 9. These are composites of 54 cases each, where the amplitude of the wind anomalies was larger than 1 m s^{-1}. The composites show an organized structure in a pattern not unlike that of the MJO. These lower tropospheric winds on the time scale of 20–60 days rotate in a clockwise sense when the earthquake occurrences swing to the north and vice versa. The largest amplitude of these low frequency winds was around 3 m s^{-1}, and the means appearing in Fig. 9 are arguably recognizable above the uncertainty of the estimate. The accuracy of the winds is of the order of 1 m s^{-1} and the accuracy of the estimates of low frequency winds are much less than 1 m s^{-1}.

A possible relationship between the length of day data sets and the earthquake frequencies is shown in Fig. 10. Here, we have averaged the filtered length of day measurements to retain the intraseasonal time scales, separately for the ascending and descending phase of our suggested western Pacific earthquake occurrence cycle. The ascending phase is where the earthquake occurrence proceeds clockwise around the western rim of the Pacific plate and the descending phase is its inverse. This separate averaging shows an increased length of day during the ascending node of earthquake frequencies and vice versa with a peak to trough amplitude on the order of 0.06 ms. Fluctuations in the length of day from the unfiltered record are of the order of a few milliseconds and the accuracy of the length of day data sets is 0.015 ms (24).

We have noted a lag of roughly 5–10 days between two low frequency zonal wind atmospheric anomalies (on the time scale of 20–60 days) and the low frequency representation of the earthquake peaks (Fig. 11). The low frequency zonal winds were extracted near the western rim of the Pacific plate over a box located between 140–150° E

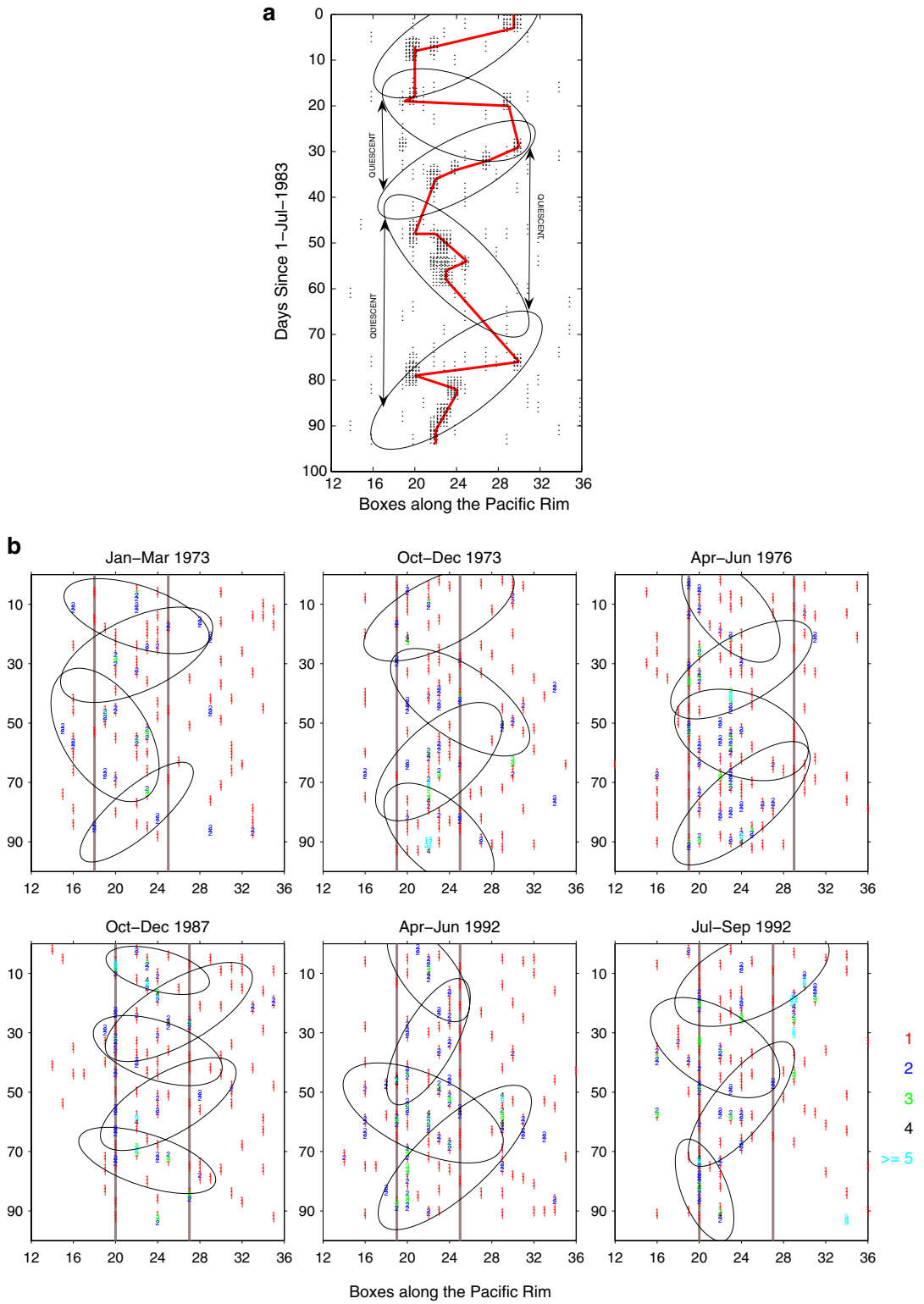

Fig. 7 **a** This is an *S–T* diagram along the western Pacific plate of earthquake activity. *S* follows the western rim and $S = 24$ denote a reference point in Indonesia with the largest activity in the last 30 years. The symbols within this *S–T* plane denote earthquake intensities. The ordinate shows 100 days of activity and the abscissa are the bins. The ellipses are schematic enclosing regions of earthquake activity. The *red line* is also schematic; it connects some of the salient earthquakes during the period June through September 1983. **b**, **c**, and **d** show further examples of the pendulum-like oscillation of earthquake activity along the western rim of the Pacific plate. The rest are same as in Fig. 7a. The *red line*, similar to that of Fig. 7a, is not illustrated here. These cover examples covering several 100-day periods between 1973 and 1997

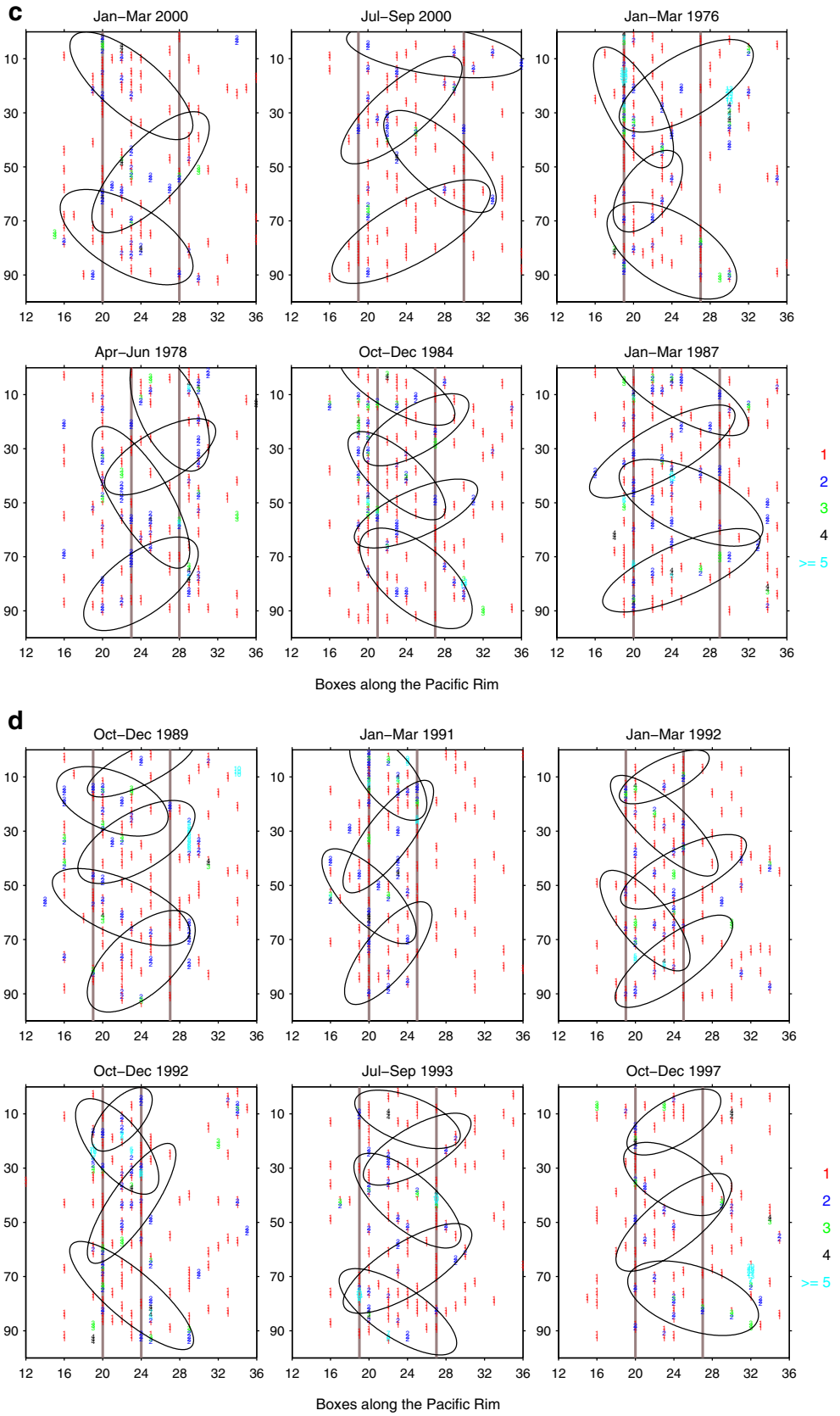

Fig. 7 continued

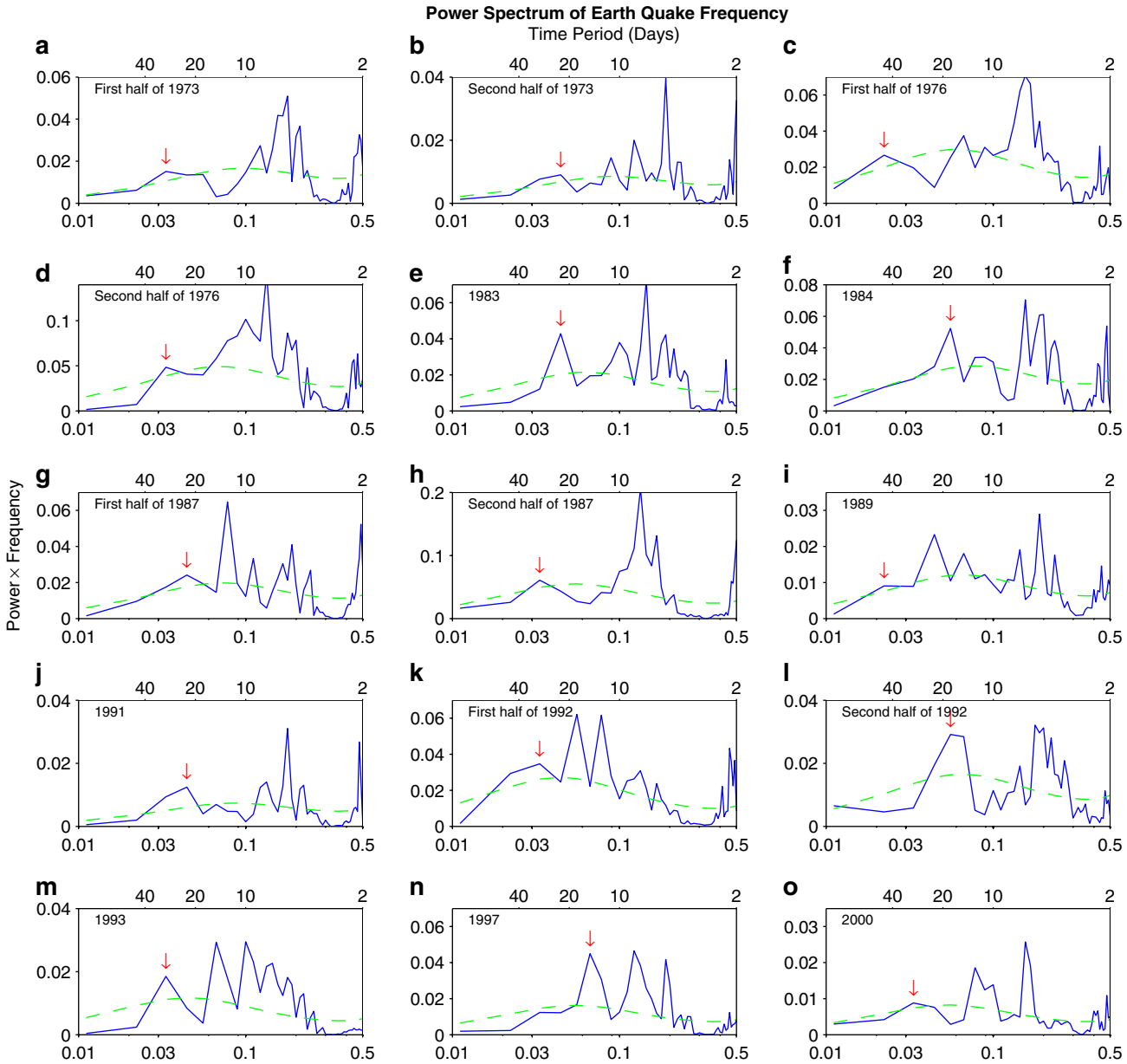

Fig. 8 Power spectra for selected years. These are power spectra for the bins 18 and 23 where the low frequency oscillations were quite evident. The ordinate denotes power times the frequency and the abscissa denotes frequency as period. The spectra of the red noise are shown by the *dashed line*. The *arrow* indicates a peak on frequency on the MJO time scale

and 10°S-EQ. The low frequency earthquake frequencies were extracted from box 24 of the western rim of the Pacific plate. The ordinate of Fig. 11 shows days after the start (day 0) of any of the seasons when a strong (>0.5 m s^{-1}) peak in the zonal wind anomaly was noted. The abscissa shows the low frequency peaks of the earthquakes with respect to the same start data of a season. After examining 36 such major peaks of earthquakes, this scatter diagram was plotted which shows an interesting phase lag, i.e., the zonal wind anomalies seem to peak roughly 10 days prior to a peak of the low frequency earthquake activity. This can be coincidental since both peaks carry low frequency representation for the same time scales. Further study is clearly warranted.

Finally, we consider simple models for communication between atmosphere and solid earth. Note that the angular momentum of the earth can be altered by frictional and mountain torques. However, the surface frictional torqueses are smaller in magnitude compared to the mountain torques (Krishnamurti et al. 1992). The change in length of day by the wind-forced mountain torques on intraseasonal time scales has been well established in the references cited below. Here, we consider the consequences on tectonic plate boundaries as the earth is spun up or spun down with each

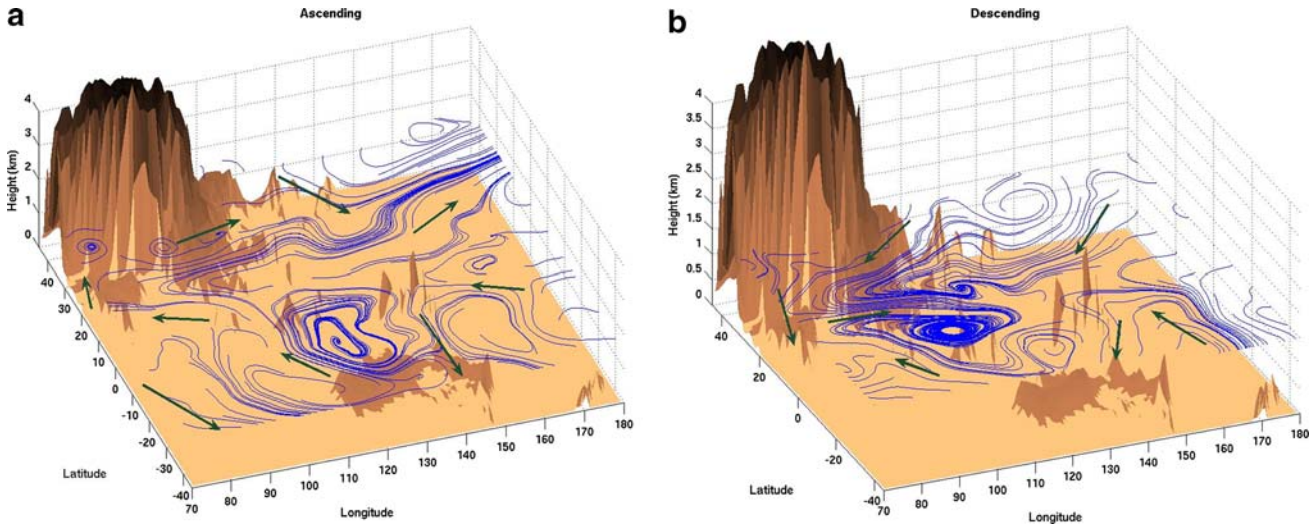

Fig. 9 This illustration shows the averaged MJO time scale circulations during two different epochs of the pendulum-like oscillation of the earthquake activity. The ascending node is when the activity is moving northwards (of bin 24) and the descending node is its converse. The topography, especially the mountain chains of East Asia and neighboring Islands, are also shown here. The circulation center and its amplitude increase during the descending node when these circulations are closer to the high mountains

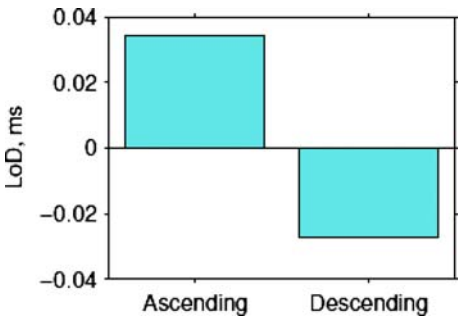

Fig. 10 The length of day anomalies in milliseconds are shown along the ordinates, and the ascending and descending modes are identified along the abscissa. These are averages based on 28-years earthquake data sets

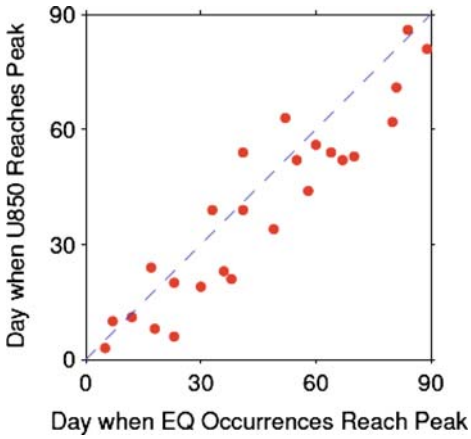

Fig. 11 This shows a scatter plot of the days when the MJO time scale wind anomalies at the 850 hPa reached a peak (along the ordinate) and the day when the earthquake occurrences reached a peak. That scatter suggests a relationship between these two parameters

change in length of day. The model is one in which the continent carrying plates with mountains that stand tall into the atmosphere effectively act as sails, giving rise to mountain torques that apply a net surface force to continental plates. Wind-induced torques on the continental Eurasian landmass transmit an oscillating force through the elastic (or visco-elastic) Eurasian plate in a direction highly oblique to the general north–south trend of the Pacific plate's convergent plate boundaries (Fig. 1b). This action would have the perturbing effect of alternately slightly increasing/decreasing the differential compressive stresses along the western Pacific plate boundaries over a 20–60 day period.

As subduction zone faults are progressively loaded with increasing stress by convergent lithospheric plate motion, isolated segments of these faults are continuously brought toward the critical threshold differential stress required for brittle failure. Triggering of Coulomb-type failure and resulting earthquake generation occurs in regions of built-up elastic stress along fault systems that are locked (stable) but have stress states close to the failure criteria. Stress redistribution due to adjacent or distant seismic events can either induce or suppress seismicity depending upon the local Coulomb stress changes (Freed 2005). Failure can be induced by either increasing the shear stress on the fault plane or by decreasing the effective normal stress on the plane. During the Pacific rim's earthquake ascending mode, the wind-induced torques on Asia could cause a slight decrease in effective normal stress on west Pacific subduction zones, thus possibly contributing to a positive Coulomb stress change resulting in failure. During the

opposite mode, the net effective normal stress increase on subduction zone faults could serve as a more efficient "clamping" stress, inhibiting earthquake activity. The force F (retrievable from the torque given by Madden and Speth (1995)) represents a time- and space-varying component to the stress field affecting subduction zone faults, since F itself varies with latitude and with time according to the MJO. However, a more detailed model is clearly needed.

4 Conclusions

The USGS data set on earthquake intensity carries global activity information on a daily basis covering several decades. A global view of this problem has not appeared much in the literature. If one tabulates the earthquake data sets using a global latitude/longitude grid on a daily basis and casts it using a spherical harmonic representation of a finite sum of waves, we find that the summed vector spectral amplitudes show a potentially important low frequency oscillation in time that is clearly evident in 32 years from the use of daily data sets. A prominent low frequency time scale of around 40 days is evident in the power spectral analysis. This is illustrated here from the distribution and time variability of the spectral amplitudes of the global earthquake data sets.

We have also shown that earthquake activity on the western rim of the Pacific plate moves alternately clockwise then counterclockwise along the rim with a time scale of 20–60 days. The pendulum-like swing has a spatial extent of roughly 10,000 km. This is a related major finding of this paper. This happens to be the same time scale found in the atmosphere and ocean called the MJO, where the wind-induced mountain torques reverse direction, and the length of day decreases and increases. An analogy to the atmospheric cloud elements of the MJO is drawn here for the earthquake cycle and its quiescent phase. This important space-time feature possibly suggests for the prediction of a space-time earthquake envelope to infer periods of activity or quiescence. The activity of individual earthquakes along given fault systems is not the goal of this study.

The MJO is a much referenced (Madden and Julian 1971, 1972; Krishnamurti et al. 1992; Wang 2006) tropical wave. It has been cited in reference to the birth and demise of the El-Nino time scale (4–6 years) phenomena (Weickmann 1991). The passage of this MJO wave clearly modulates the amplitude of the monsoon westerlies and the trade wind easterlies (Waliser 2006). This passage of MJO waves over the western Pacific Ocean modulates typhoon tracks (Chan 2000) and tropical cyclone activity (Hall et al. 2001). More recently, we have mapped the passage of this wave in the sub-surface oceans (Krishnamurti et al. 2007). Atmospheric scientists have carried out extensive studies on estimating mountain torques over the globe (Lott et al. 2001). The 1–2 weeklong persistent MJO winds with amplitude of the order of 3–5 m s^{-1} at the earth's surface can communicate such torques to the mountain chains of Asia. Those data sets of the mountain torques do carry pronounced signals on the MJO time scale (Newton 1971; Dickey et al. 1991; Iskenderian and Salstein 1998). Future research on the global scale earthquake amplitude variation and the relationships among the pendulum-like swings of the earthquake frequencies on the western rim of the Pacific plate to the atmosphere-ocean phenomena on those same scales would be very worthwhile.

Acknowledgments We acknowledge NSF grants ATM-0419618, OCE-242535 and OCE-0424227.

References

Aki K (1996) Scale dependence in earthquake phenomena and its relevance to earthquake prediction. Proc Natl Acad Sci 93:3740–7347

Chan JCL (2000) Tropical cyclone activity over the western North Pacific associated with El Nino and La Nina events. J Climate 13:997–1004

Dickey J, Ghil M, Marcus S (1991) Extratropical aspects of the 40–50 day oscillation in length-of-day and atmospheric angular momentum. J Geophys Res 96:22643–22658

Freed A (2005) Earthquake triggering by static, dynamic, and postseismic stress transfer. Annu Rev Earth Planet Sci 33:335–368

Gret A, Snieder R, Scaled J (2006) Time-lapse monitoring of rock properties with coda wave interferometry. J Geophys Res 111. doi:10.1029/2004JB003354

Hall JD, Matthewsb AJ, Karoly DJ (2001) The modulation of tropical cyclone activity in the Australian region by the Madden-Julian Oscillation. Mon Weather Rev 129:2970–2982

Iskenderian H, Salstein DA (1998) Regional sources of mountain torque variability and high frequency fluctuations in atmospheric angular momentum. Mon Weather Rev 126:1681–1694

Kanamori H (1981) In: Simpson DW, Richards P (eds) Earthquake prediction an international review. American Geophysical Union, Washington, DC

Knopoff L (1996) Earthquake prediction: the scientific challenge. Proc Natl Acad Sci 93:3719–3720

Krishnamurti TN, Sinha MC, Krishnamurti R, Oosterhof D, Comeaux J (1992) Angular momentum, length of day and monsoonal low frequency mode. J Meteorol Soc Jpn 70:131–166

Krishnamurti TN, Chakraborty A, Krishnamurti R, Dewar WK, Clayson CA (2007) Passage of intraseasonal waves in the subsurface oceans. Geophys Res Lett 34:L14712. doi:10.1029/2007GL030,496

Lott F, Robertson AW, Ghil M (2001) Mountain torques and atmospheric oscillations. Geophys Res Lett 28:1207–1210

Madden RA, Julian PR (1971) Detection of a 40–50 day oscillation in the zonal wind in the tropical pacific. J Atmos Sci 28:702–708

Madden RA, Julian PR (1972) Description of global-scale circulation cells in the tropics with a 40–50 day period. J Atmos Sci 29:1109–1123

Madden RA, Speth P (1995) Estimates of atmospheric angular momentum, friction, and mountain torques during 1987–1988. J Atmos Sci 52:3681–3694

Nakazawa T (1988) Tropical super cloud clusters within intraseasonal variations over the western pacific. J Meteorol Soc Jpn 66:823–839

Namias J (1988) Similarity of anomalous sea level pressure fields during the July 1986 and September 1987 southern California quakes—accidental or indicative & quest. Geophys Res Lett 15(4):350–352

Namias J (1989) Summer earthquakes in southern California related to pressure patterns at sea level and aloft. J Geophys Res 94(B12):17671–17679

Newton CW (1971) Mountain torques in the global angular momentum balance. J Atmos Sci 28:623–628

Sykes LR (1996) Intermediate- and long-term earthquake prediction. Proc Natl Acad Sci 93:3732–3739

Waliser DE (2006) Intraseasonal variability. In: Wang B (ed) The asian monsoon. Springer, Heidelberg, pp 203–257

Wang B (Ed) (2006) The asian monsoon. Springer, Heidelberg

Weickmann KM (1991) El Nino/Southern Oscillation and Madden-Julian (30–60 day) oscillations during 1981–1982. J Geophy Res 96:3187–3195